THE JOURNAL OF PHYSICAL CHEMISTRY C

Article

Cite This: J. Phys. Chem. C 2019, 123, 16711−16720

pubs.acs.org/JPCC

Preferential Adsorption in Mixed Electrolytes Confined by Charged Amorphous Silica

Max F. Döpke,[†] Johannes Lützenkirchen,[‡] Othonas A. Moultos,[†] Bertrand Siboulet,[§] Jean-François Dufrêche,[§] Johan T. Padding,[†] and Remco Hartkamp*[,†]

[†]Process & Energy Department, Delft University of Technology, Leeghwaterstraat 39, 2628 CB Delft, The Netherlands

[‡]Institut für Nukleare Entsorgung, Karlsruher Institut für Technologie, P.O. Box 3640, 76021 Karlsruhe, Germany

[§]Institut de Chimie Séparative de Marcoule ICSM, UMR 5257 CEA, CNRS, ENSCM, Université Montpellier, Bâtiment 426, F-30207 Bagnols-sur-Cèze, France

Supporting Information

ABSTRACT: Preferential ion adsorption in mixed electrolytes plays a crucial role in many practical applications, such as ion sensing and separation and in colloid science. Using all-atom molecular dynamics simulations of aqueous NaCl, $CaCl_2$, and NaCl−$CaCl_2$ solutions confined by charged amorphous silica, we show that Na^+ ions can adsorb preferentially over Ca^{2+} ions, depending on the surface structure. We propose that this occurs when the local surface structure sterically hinders the first hydration shell of the Ca^{2+} ion. Introducing a protrusion metric as a function of protrusion of deprotonated silanols, ion-specificity is successfully predicted on isolated, vicinal, and geminal silanols alike, provided that no other deprotonated silanols are found nearby. Furthermore, we introduce a new strategy to analyze the results as a function of distance from the surface. This approach effectively removes surface roughness effects allowing for direct comparison with classical electric double layer theory and distinction of specifically adsorbed ions and electrostatically adsorbed ions.

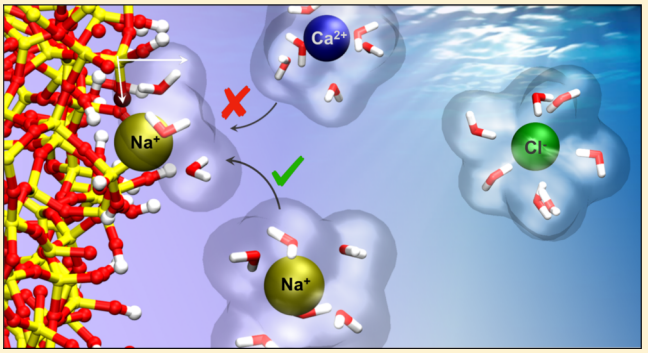

1. INTRODUCTION

Most fluids in nature are complex aqueous solutions containing multiple electrolytes, possibly in combination with other organic and inorganic compounds. The nanoscale properties of these mixtures at fluid−solid interfaces can be exploited for applications such as soil analysis, ion separation, and water purification.[1−3] Silica surfaces are among the most widely studied, due to their omnipresence in nature, their bimodal chemical character,[4] and their use in a wide range of applications,[5−7] including catalysis[8] and ion sensing.[9,10]

Oxide surfaces in contact with aqueous solutions assume an electric charge as a result of protonation and deprotonation of ionizable groups.[11] The silica surface is negatively charged above the point of zero charge ($pH_{pzc} \approx 2-3$),[12] attracting cations whilst repelling anions, forming a so-called electrical double layer (EDL). The exact distribution and movement of ions and solvent molecules in the EDL determine, for example, transport along the surface and charge storage at the surface. However, no single experimental technique can unambiguously measure the three-dimensional distribution, orientation, and motion of molecules constituting the fluid. In theory, the full picture could be constructed by combining the partial information inferred from multiple techniques, but it is difficult to replicate identical environmental conditions and samples in different experimental setups. Moreover, various techniques (e.g., atomic force microscopy, titration, and electrokinetic techniques) rely on fitting measurement data to EDL models (e.g., Gouy−Chapman−Stern−Grahame[13] shown in Figure 1) to infer quantities that cannot be directly measured. Such models are based on a priori assumptions, such as that the solid surface is flat and homogeneous, fluid transport coefficients are constant in space, and the Stern and diffuse layers are distinct. These assumptions may be suitable only under certain idealized conditions, thus limiting the accuracy and interpretation of inferred quantities for most systems of interest.[14]

A bottom-up approach, such as molecular dynamics (MD) simulation, can provide detailed insight into molecular structure and dynamics at the nanoscale. Various EDL properties can be directly and locally calculated from the position and motion of atoms, without the need for an EDL model to infer information. As such, molecular simulations offer an appealing alternative approach to gain detailed insight into EDL properties. Furthermore, insight from MD

Received: March 29, 2019
Revised: May 23, 2019
Published: June 18, 2019

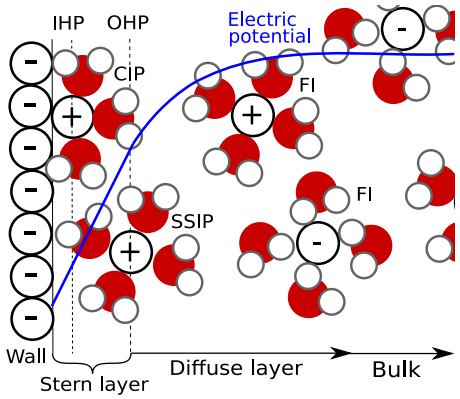

Figure 1. Gouy–Chapman–Stern–Grahame EDL model on smooth surfaces, with the Stern and diffuse layer, and the bulk region. The Stern layer is delimited by the outer Helmholtz plane (OHP), passing through the nuclei of solvent-separated ion pairs (SSIP), whereas an inner Helmholtz plane (IHP) passes through contact ion pairs (CIP). Ions beyond the OHP are free ions (FI).

simulations can aid in improving the models used to interpret experimental observations.[14]

Numerous MD studies have expanded our knowledge of interfacial fluid phenomena on silica surfaces in recent years. For example, water structure and dynamics on crystalline silica were studied extensively by Argyris et al.,[15,16] and on amorphous silica, by Hassanali et al.[17,18] and Bourg and co-workers.[19,20] With water–silica interfaces better understood, the focus has shifted toward the simple, single compound, electrolyte–silica interfaces.[3,19,21−30] For example, Haria et al.[23,24] found that charged amorphous silica nanopores show selectivity for ions to enter depending on the pore size and ionic and hydration radii. Ionic and hydration radius-based adsorption selectivity on β-cristobalite was also observed by Ho et al.,[26] who suggested that ion–surface and ion–water interactions dominate over ion–ion interactions for NaCl or CsCl systems. Recently, Hartkamp et al.[29] found that adsorption follows a reversed Hofmeister series, $Na^+ < K^+ < Cs^+$, with the smallest ion adsorbing closest to the surface, and the largest the furthest away. This effect was attributed to the ionic radius, but may in fact better be seen in terms of the hydration radius. Later, using the McMillan–Mayer potential of mean force (PMF), Hocine et al.[28] calculated the binding energy of Li^+ and Cs^+ on amorphous silica and found much stronger binding energy for Li^+, and correspondingly a much longer adsorption residence time.

Although molecular simulations have contributed to an improved understanding of solid–electrolyte interfaces, many studies have suffered from drastic simplifications pertaining to the representation of the surface, the solvent or the electrolyte. With regard to the surface, many studies have considered smooth model surfaces.[31,32] Furthermore, most MD studies make use of rigid surfaces, limiting mobility induced by the vibration of surface atoms, which can influence adsorption properties as well as slip along a surface.[33] The working fluid in most MD simulation studies has been an aqueous solution of simple, monovalent electrolytes, such as NaCl or KCl, whereas most solutions in nature and industry contain a mix of electrolytes. Experimentally,[10,34,35] it has been shown that adding even a small amount of different ions to an electrolyte solution can severely impact EDL properties. This can occur, for example, if the added electrolytes show preferential adsorption or if they severely affect the hydrogen bond network of the solvent at the interface. In particular, the addition of multivalent ions to a predominantly monovalent solution can strongly reduce the efficiency of reverse electrodialysis[36] and can invert the direction of electrokinetic flow.[35]

The first fully atomistic MD simulations of electrolyte mixtures on siliceous surfaces were carried out by Bourg and Sposito[3] in 2011, who investigated NaCl–$CaCl_2$ mixtures on a rigid smectite surface and found that Na^+ and Ca^{2+} ions can coexist in the Stern layer, with no clear preferential adsorption. In similar MD simulations on rigid mica surfaces, however, preferential adsorption of K^+ over Rb^+ and Mg^{2+} was found.[37] Cavities in which K^+ ions could adsorb were not accessible to Rb^+ and Mg^{2+} ions, which have larger hydration radii. To our knowledge, only one MD study has considered mixed electrolytes on amorphous silica. Prakash et al.[30] evaluated electro-osmotic flow on a rigid amorphous silica surface at varying compositions of NaCl–$MgCl_2$ solutions, stating that Na^+ preferentially adsorbs over Mg^{2+}. This was motivated by the fact that Na^+ displayed closer proximity to the surface and has a lower hydration energy than Mg^{2+}. However, the balance between adsorption energy and hydration energy was not considered. Furthermore, we argue that the closer proximity of Na^+ ions does not demonstrate preferential adsorption, but rather is a consequence of its smaller hydration radius. Conversely, a recent primitive model Monte Carlo study suggested that divalent ions adsorb preferentially over monovalent ions when discrete charges are present on a model surface.[38] A comprehensive study of ion adsorption with mixed electrolytes on realistic amorphous silica surfaces is lacking.

In this article, we provide one of the first studies of ion adsorption from mixed electrolytes confined by flexible charged amorphous silica. Adsorption of ions in single and mixed electrolytes is compared by analyzing the distribution of ions near a charged silica surface. Specifically, ions are classified based on their adsorption, forming a contact ion pair (CIP) or solvent-separated ion pair (SSIP) with the surface (see Figure 1), to assess the impact of adsorption type on the EDL structure. This classification is analogous to inner- and outer-sphere surface complexes used by, for example, Bourg et al.[3] Furthermore, the strong influence of the surface roughness on the EDL structure is illustrated by computing for each ion the distance to the nearest surface atom. Finally, we provide selectivity maps for our system, and relate the observed selectivities to the structural characteristics of the surface, allowing us to devise a protrusion metric (PM) based on steric properties, which is successfully used to predict ion-specificity.

The remainder of this article is organized as follows: the simulation set-up is described in Section 2. The results are given in Section 3 discussing adsorption of ions in single (one compound) and mixed (multiple compounds) electrolytes. Conclusions are presented in Section 4.

2. METHODS

A block of 5 nm × 5 nm × 5 nm amorphous silica was created by annealing and quenching β-cristobalite using a modified van Beest–Kramer–van Santen potential[39−41] described in Section S2.1 of the Supporting Information (SI). In summary, an annealing temperature of 4000 K and cooling rate of 2.5 K/ps were used. The density of the amorphous silica was fixed to 2.2 g/cm^3 by performing the simulations in the NVT ensemble

DOI: 10.1021/acs.jpcc.9b02975
J. Phys. Chem. C 2019, 123, 16711−16720

(i.e., constant number of particles, volume, and temperature) with periodic boundary conditions. The temperature was controlled with the Nosé−Hoover thermostat. A simulation time step of 1 fs and a temperature damping factor of 100 fs were used. The obtained amorphous silica structure is in line with experiments[42−44] and with previous MD studies.[23,40,45,46] Amorphous silica characterization is further discussed in Section S3 in the SI.

A channel configuration was generated by cutting the amorphous silica block and separating the two resulting slabs (Figure 2). Subsequently, undercoordinated silicon and

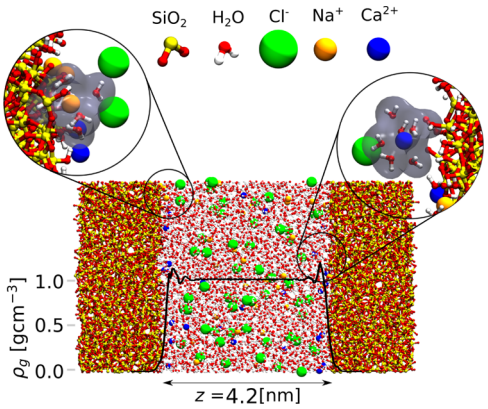

Figure 2. Channel configuration for simulations. Silica walls are separated roughly 4.2 nm with fluid in between at a density of ≈1 g/cm^3. The left inset shows Na^+ adsorption with part of the hydration shell penetrating into the wall. The right inset shows adsorption of a partially hydrated Ca^{2+} ion.

uncoordinated oxygen atoms were removed. Undercoordinated oxygen atoms were protonated, resulting in a silanol (SiOH) density of 6.5 SiOH/nm^2. The silanol density was reduced to 5 SiOH/nm^2 (close to the experimental value[47]) by condensation of silanols.[48] Condensation of vicinal silanol pairs was avoided to ensure that no strained two-membered siloxane rings were formed.[49,50] The remaining surface groups consisted of 15% isolated, 50% vicinal, and 35% geminal silanols, in line with other studies of amorphous silica[47] (see Figure 3 for a

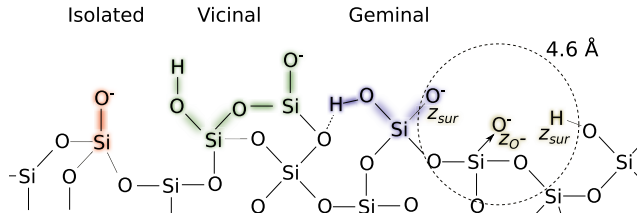

Figure 3. Silanol classification for isolated (red), vicinal (green), and geminal (blue) silanols. In yellow is shown how the protrusion metric (PM) is computed considering surface atoms within 4.6 Å, of z_{O^-}.

representation of the silanol types). On either wall, 16 SiOH were deprotonated to impose a surface charge of −103 mC/m^2, corresponding to a pH of 7−8 (depending on electrolyte composition and concentration).[11]

In between the resulting slabs, 3485 water molecules were added in a dilute lattice, along with a variable number of ions (Cl^-, Na^-, and Ca^{2+}, listed in Table 1), with an excess of cations to balance the surface charge (see Figure S1 in the SI). The fluid density was adjusted via a compression force

Table 1. Electrolyte Compositions Used in This Study with Final Densities and Molarities at the Center of the Channel in a 4 Å bin[a]

	number of ions				molarity (mol/L)	
name	Cl^-	Na^+	Ca^{2+}	density (g/mL)	NaCl	$CaCl_2$
0.1Na	6	38		1.001(4)	0.16(1)	
0.3Na	19	51		1.006(5)	0.35(1)	
0.6Na	38	70		1.019(4)	0.67(1)	
0.9Na	57	89		1.029(5)	0.91(2)	
0.15Ca	18		25	0.996(5)		0.10(1)
0.3Ca	38		35	1.011(5)		0.27(1)
0.3Na0.15Ca	38	34	18	1.014(5)	0.32(2)	0.14(1)
0.3Na0.3Ca	56	34	27	1.033(6)	0.40(2)	0.25(1)

[a]The excess of counterions can be calculated from the difference between anions and cations forming a molecule.

equivalent to 1 bar by moving the walls toward each other for 10 ns,[51] resulting in the channel configuration shown in Figure 2 with a width of approximately 4.2 nm. The electrolyte compositions used in this study are provided in Table 1, with molarities in the center of the channel computed after adjusting the fluid.

The channel simulations were performed in the NVT ensemble with periodic boundary conditions, removing interactions across the z boundary,[52] with a time step of 1 fs. The Nosé−Hoover thermostat was used to control the temperature with a damping factor of 100 fs. Long-range electrostatic interactions were computed with the particle−particle particle−mesh method with a relative precision of 10^{-4}. Cut-off distances of 12 and 8.5 Å were used for Lennard-Jones (LJ) and Coulombic interactions, respectively. The Lorentz−Berthelot mixing rules were used to parametrize LJ interactions between dissimilar particles. The interface force field (IFF) parametrization from Emami et al.[45] was used for silica, TIP4P/2005[53] for water, and Joung and Cheatham[54] and Mamatkulov et al.[55] for ions. An overview of the force field parameters and functional forms is provided in Section S2.2 in the SI. The IFF has been shown to provide physically and chemically very consistent parameters compared to other force fields that are commonly used to model silica, such as clayFF.[56−58] Furthermore, flexible silica walls can be easily simulated with the IFF due to the presence of bond and angle parameters. Despite IFF being parametrized together with TIP3P and SPC, TIP4P/2005 was chosen for water due to the fact that this model more accurately reproduces a range of physical and thermodynamic properties.[59] Oxygen−hydrogen (OH) bond lengths and HOH angles were constrained with the SHAKE algorithm.[60] All simulations in this study were performed with the large-scale atomic/molecular massively parallel simulator (LAMMPS) package.[61]

Two independent simulations of 35 ns were performed for each system given in Table 1. The last 25 ns were used to gather statistics at 5 ps intervals. An additional simulation of 122 ns was performed for the 0.3Na0.3Ca system to study ion selectivity at the surface. Runs of 11 ns were alternated with runs of 10 ps with charges switched to $q_{Na} = -0.5$, $q_{Ca} = -0.5$ and $q_{Cl} = +1.116$. This modification in ionic charges was found to be sufficient to quickly desorb the adsorbed ions, such that an independent configuration can be obtained. This process was repeated 11 times, gathering statistics throughout the last 1

DOI: 10.1021/acs.jpcc.9b02975
J. Phys. Chem. C 2019, 123, 16711−16720

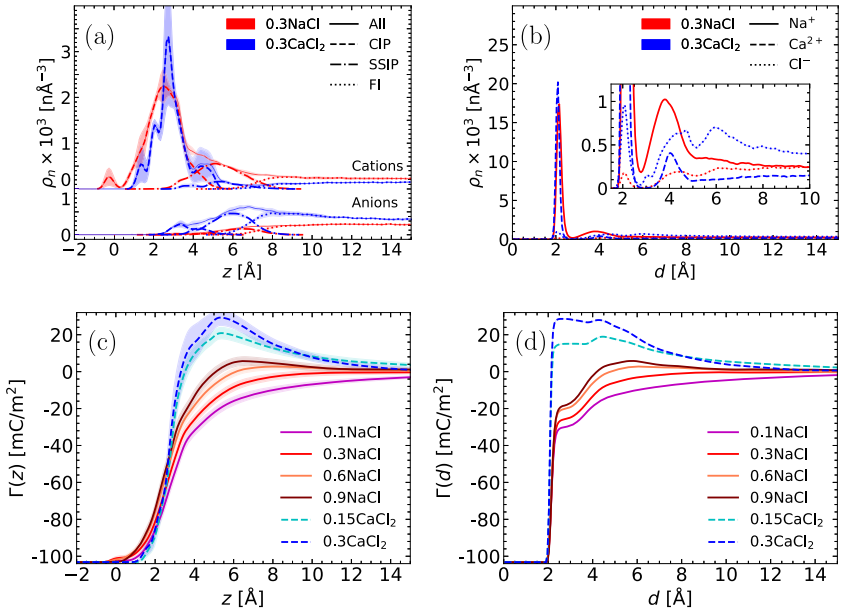

Figure 4. Number density profiles (a, b) and screening function (c, d) for single NaCl and $CaCl_2$ electrolytes as a function of z, normal to the surface (a, c), and d, distance to the nearest surface atom (Si, O, or H) (b, d). The colors in subfigures (a) and (b) indicate the electrolyte solution; NaCl (red) or $CaCl_2$ (blue). The line type indicates the ion type; Na^+ (—), Ca^{2+} (– –), and Cl^- (---). In subfigures (a) and (c), $z = 0$ is the average z-coordinate of all surface oxygen atoms. The shaded areas in all figures represent the uncertainty using 1 standard deviation (50% confidence interval). Density profiles of additional electrolyte compositions are provided in the SI.

ns of each 11 ns segment. Uncertainty quantification for the results was carried out as discussed in Section S4 in the SI.

3. RESULTS

In this section, the adsorption of ions in single and mixed electrolytes is evaluated. First, single electrolyte results are discussed, followed by a comparison with mixed systems. The section is concluded by evaluating ion-specificity of charged surface sites.

3.1. Single Electrolytes. Figure 4a shows the symmetrized cation density (top) and anion density (bottom) near the charged silica surface as a function of z, the coordinate normal to the surface. Symmetrizing of density profiles is briefly discussed in Section S5 in the SI. A dense layer of Na^+ and Ca^{2+} is found near the surface, with most adsorbed ions forming CIPs (dashed lines). Ions forming CIPs plus those forming SSIPs make up the Stern layer, which here is found to have a thickness of approximately 8 Å, in line with experimental estimates, 6–10 Å.[62] CIPs are formed when water molecules in the first hydration shell of the ion are replaced by a surface atom (Si, O, or H), and SSIPs are formed when this occurs in the second hydration shell. The first and second hydration shells are commonly delimited by the first and second minima in the ion–water radial distribution function (rdf), respectively. The properties of the first hydration shell can be used to explain why Na^+ ions are found closer to the surface than Ca^{2+} ions. Let us consider the first maximum of the ion–water rdf to compute the ion hydration density ($H_2O/Å^2$). For TIP4P/2005, the maxima were found to be at 2.375 and 2.5 Å (see Hartkamp and Coasne[63] and Figure S2 in the SI), giving a hydration density of 0.0846 and 0.102 $H_2O/Å^2$, with six and eight water molecules in the first hydration shell, for Na^+ and Ca^{2+}, respectively. This indicates that Na^+ ions have a less tight hydration shell (e.g., fewer water molecules per hydration shell surface area) than Ca^{2+} ions. This allows water molecules to shift within the hydration shell of Na^+ ions, enabling these to move closer to the surface than Ca^{2+} ions.[63] Consequently, adsorbed Ca^{2+} ions display a larger change in coordination number, ΔCN, than adsorbed Na^+ ions, as discussed in more detail in Section 3.3.

The difference in the distance from the surface for different ions is not accounted for in classical EDL theory. In theory, different ions would need to be assigned their own electrostatic planes,[64] the inner Helmholtz plane (IHP) and the outer Helmholtz plane (OHP) (see Figure 1), defined as passing through the centers of CIP and SSIP, respectively.[65] This, however, proves to be very elaborate for multicomponent systems. Furthermore, even a root-mean-squared (rms) surface roughness of 1.1 Å, (experimentally reported values vary from 0.2 up to several nanometers),[66] obtained from the rms of the CIP z-position, can be shown to severely impact the suitability of EDL theory. In Figure 4a, no distinct planes can be found for any of the ionic species. Instead, the figure shows overlapping regions in which CIP and SSIP coexist. Density profiles as a function of z strongly depend on the surface roughness, causing the density profiles to be highly specific to the characteristics of the surface. This specificity is also responsible for the large error margins near the surface. Part of this specificity can be eliminated when considering the density as a function of the distance, d, to the nearest wall atom (Si, O, or H). This measure provides an effective means to decouple the effect of surface roughness from ion specific properties such as the adsorption state, which can more easily be identified in this way. Similarly, one could say that the density as a function of d closely resembles the density profile as it would occur on a perfectly smooth surface with localized surface sites. Indeed, the density profiles in Figure 4b are found to closely resemble those found for smooth surfaces (see, for example, refs 67, 68), and provide a clear distinction of atom layers corresponding to CIP and SSIP by the minima at $d \approx 3$

DOI: 10.1021/acs.jpcc.9b02975
J. Phys. Chem. C 2019, 123, 16711–16720

Å. Furthermore, this representation is in line with the classical definition of IHP and OHP for each ionic species, as passing through the centers of CIP and SSIP.

Different from Figure 4a, in Figure 4b, Na^+ ions and Ca^{2+} ions are found at similar distances from the surface. Additionally, the presence of Cl^- ions forming CIP is highlighted in this representation, in line with some experimental observations.[69] In the inset of Figure 4b, a strict distinction of CIP and SSIP for Ca^{2+} ions is observed, whereas Na^+ ions are also found in an adsorption state that is neither strictly defined as CIP nor SSIP. This can be interpreted as Ca^{2+} ions having distinct preferred distances to form CIP and SSIP, suggesting a clear energy barrier between CIP and SSIP. On the other hand, Na^+ ions can also occupy adsorption states between CIP and SSIP, indicating a lower free energy barrier between these adsorption states. Finally, the local excess of Cl^- ions, immediately following the SSIP region in the $CaCl_2$ solution, indicates the occurrence of overscreening or charge inversion (CI), discussed in more detail below.

We define a screening function $\Gamma(\chi)$ to indicate the screening of the surface charge by the ions up to χ as the sum of bare surface charge σ_0 and the integral over the ion number density $\rho_{n,i}$ multiplied by the ion valency Z_i for ion type i as[3]

$$\Gamma(\chi) = \sigma_0 + \int_{\min(\chi)}^{\chi} \sum_i \rho_{n,i}(\chi') Z_i \, \mathrm{d}\chi' \tag{1}$$

with χ being a placeholder for z or d. Note that $\Gamma(d)$ differs from a radial distribution function because only the distance to the nearest surface atom is considered for each ion. A surface is considered fully screened when the screening function approaches zero. Figure 4c,d shows Γ as a function of z (c) and d (d), obtained by applying eq 1 to the ion density profiles. As the ion concentration increases, the diffuse region becomes more compact due to a shorter Debye length. Consequently, the EDL thickness is reduced. This behavior has also been reported by others, based on streaming current measurements[35] and X-ray photoelectron spectroscopy.[62] For NaCl, the contributions of CIP ($d \leq 2.75$) and SSIP ($2.75 < d \leq 5.5$), both increase at increasing concentration, whilst for $CaCl_2$, only the CIP contribution increases. In fact, for NaCl, we can find a linear trend of $0.03 \times \sigma_0$ increase in screening for each 0.3 M increase (see also Figure 5). The screening function for the 0.9Na and both $CaCl_2$ systems exceeds zero, indicating overscreening or CI. This phenomenon occurs when an excess of counterions is attracted to the surface, changing the sign of Γ. For NaCl, CIP and SSIP appear to contribute equally to CI.

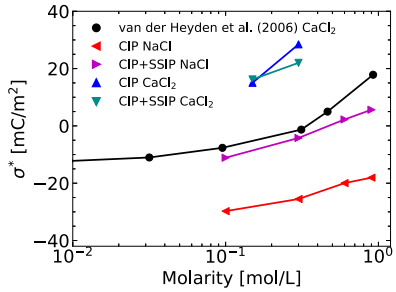

Figure 5. Effective surface charge σ^* for NaCl and $CaCl_2$ considering CIP and CIP + SSIP. The lines are added as a guide for the eye.

On the other hand, for $CaCl_2$, CIP contributes to a greater extent to CI than SSIP.

van der Heyden et al.[35] inferred the effective surface charge from streaming current measurements as $\sigma^* = \sigma_0 + \rho_{n,\mathrm{Stern}} Z_i$, where the Stern layer is considered to be composed of immobile ions yielding $\sigma^* = \Gamma(d = d_{\mathrm{immobile}})$, with d_{immobile} representing the distance from the surface up to where ions are considered immobile. The bare surface charge density of fused silica at pH = 7.5 was estimated as -150 mC/m^2, and the authors interpreted their measurements assuming no-slip Poiseuille flow and Boltzmann charge distribution. Their result is included in Figure 5, showing a sign reversal at 0.4 M $CaCl_2$. This method of determining CI only considers immobile ions, which are often considered to include the entire Stern layer, e.g., CIP and SSIP. Relative to the results of van der Heyden et al., our MD results overpredict the occurrence of CI for $CaCl_2$. The effective surface charge estimated from electrokinetic experiments can deviate from what would be observed in MD, due to multiple factors: first, the simulation force field is not optimized for dynamic properties; second, the effective surface charge is inferred from streaming current measurements using multiple assumptions that may be inaccurate. Furthermore, the effect of fluidic transport on charge distribution is debated. Some authors[70,71] have claimed that fluidic transport can alter the charge distribution, which would result in a nonlinear electrokinetic response. In contrast, our previous work[72] has shown linear electrokinetic response in electro-osmotic flow with electric fields up to 25×10^6 V/m ($O(1-10^3)$ V/m is characteristic for electrokinetic experiments).[73,74] Consequently, the relationship between CI and electro-osmotic flow reversal may not be unique.

In many numerical studies, the occurrence of CI is underpredicted due to the use of uniformly charged model surfaces. These surfaces have been shown to predict less CIP formation, which is crucial for accurate predictions of CI.[31,38,67,75] In fact, CI has been argued to be a discrete phenomenon which strongly depends on specific ion adsorption.[38,75] For example, on a discretely charged wall, CI occurs locally when a higher valency ion or multiple monovalent ions adsorb to a SiO^-. For monovalent ions, this behavior has been observed in previous MD simulations[10] and is confirmed by our results (see Table S1 in the SI). On the other hand, various numerical studies using discrete charges have overpredicted the occurrence of CI due to the force fields used.[22,29,76,77] For example, the silica parametrization of clayFF[56,57] contains neither bond nor angle parameters, requiring higher partial charges, which can lead to unphysically strong electrostatic interactions. Furthermore, we note that the Ca^{2+} parametrization used in this study has some known deficiencies,[78] but no better parameters exist at the present time.

3.2. Mixed Electrolytes. By combining the ions from single 0.3Na with 0.15Ca or 0.3Ca systems in the mixed 0.3Na0.15Ca and 0.3Na0.3Ca systems (see Table 1), the total ionic concentration increases. This reduces the EDL thickness, in part due to a shorter Debye length. However, it is not obvious which ions would adsorb and how these distribute within the Stern layer. These matters will be investigated in the following.

Figure 6 includes the density profiles and screening functions for the single 0.3Na, 0.3Ca, and the mixed 0.3Na0.3Ca systems. Figure 6a shows how Na^+ adsorption

DOI: 10.1021/acs.jpcc.9b02975
J. Phys. Chem. C 2019, 123, 16711−16720

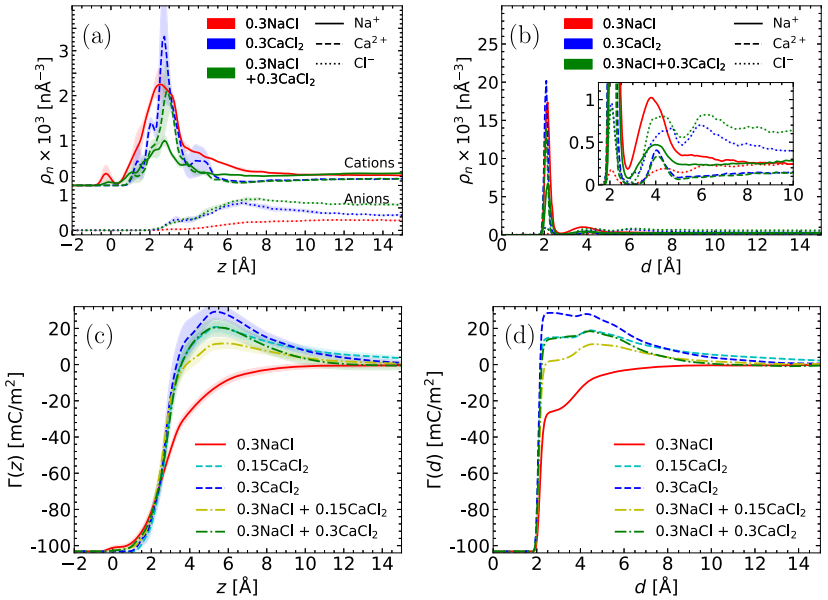

Figure 6. Number density profiles (a, b) and screening function (c, d) for single NaCl and $CaCl_2$ and mixed NaCl−$CaCl_2$ electrolytes as a function of *z*, normal to the surface (a, c), and *d*, distance to the nearest surface atom (Si, O, or H) (b, d). In subfigures (a) and (b), the colors indicate the electrolyte solution; NaCl (red), $CaCl_2$ (blue), or NaCl + $CaCl_2$ (green). The line type indicates the ion type; Na^+ (—), Ca^{2+} (– –), and Cl^- (---). In subfigures (a) and (c), $z = 0$ is the average location of all surface oxygen atoms. The shaded area in all figures represents the uncertainty using 1 standard deviation (50% confidence interval). Density profiles of additional electrolyte compositions are provided in the SI.

(CIP + SSIP) in the mixture is reduced by more than 50% compared to the single electrolyte solution, while Ca^{2+} adsorption is only reduced by 30%. Stronger Coulombic attraction is expected for Ca^{2+} ions than for Na^+ ions, based on the higher partial charges of the former. Despite this, we find Na^+ ions adsorb closest to the surface. When the surface structure near dangling oxygen provides steric hindrance to the hydrated ion, additional water molecules need to be expelled from or shifted within the first hydration shell of the ion. Since Na^+ ions have a less tight hydration shell than Ca^{2+} ions (see the discussion above), these can shift water molecules around more easily than Ca^{2+} ions and hence adsorb with fewer water molecules being rejected from its hydration shell ions as shown in Figure 8b. The results of this preferential adsorption are shown in the insets in Figure 2. On the left, an adsorbed Na^+ ion is shown to penetrate the surface with part of its hydration shell, whilst on the right, an adsorbed hydrated Ca^{2+} ion is shown to remain superficial. This preferential adsorption behavior between Na^+ and Ca^{2+} leads to a reduction in CIP formation for Ca^{2+} in mixed compared to single electrolytes, as seen in Figure 6a,b. Consequently, also the CIP contribution toward surface screening is reduced from 129.3 mC/m² in the 0.3Ca system to 115.3 mC/m² in the 0.3Na0.3Ca system and from 123.9 mC/m² in the 0.15Ca system to 111.5 mC/m² in the 0.3Na0.15Ca system as shown in Figure 6d. In terms of SSIP formation in Figures 6b and S8, a consistent reduction of Na^+ and Ca^{2+} ions is observed in the mixed systems compared to the single systems. Changes in Cl^- SSIP formation, however, are not consistent across the mixed systems studied. Upon comparing the 0.15Ca to the 0.3Na0.15Ca system, an increase of Cl^- SSIP formation is observed, whereas upon comparing the 0.3Ca to the 0.3Na0.3Ca system, a decrease is observed. Nonetheless, the SSIP contribution is small compared to the CIP contribution toward the surface screening for the mixed and single $CaCl_2$ systems, resulting in a consistent reduction of overall surface screening and CI when adding monovalent ions to a divalent solution.

The above behavior of preferential adsorption and CI reduction is consistent with experiments that suggested a reduction of multivalent ion adsorption upon addition of monovalent ions.[35,79−82] For example, van der Heyden et al.[35] measured a reduction and even sign reversal of current in streaming current experiments for a multivalent ionic solution by addition of varying amounts of monovalent ions. This was interpreted as the result of competitive effects between ions in the Stern layer. In line with these experiments, we observe surface structure-induced competitive effects in the formation of CIP and SSIP.

3.3. Surface-Induced Ion-Specificity. An additional simulation for the 0.3Na0.3Ca system was carried out as specified in the Section 2. Ions were repeatedly forced to desorb and subsequently equilibrated to adsorb, obtaining 11 uncorrelated sets of adsorbed ions. Averaging over these results, it was found that some dangling oxygens showed preferential adsorption of Ca^{2+} ions and others of Na^+ ions. Figure 7 shows the preferential adsorption found for the left and right walls. The color scale intensity goes from Ca^{2+} adsorbed in all 11 independent results (blue) to Na^+ adsorbed in all 11 independent results (red). The highest rates of preferential adsorption observed in our simulations were 64% for Ca^{2+} (7/11) and 64% for Na^+ (7/11). Roman numbers I−VI in the figure indicate regions that are specifically discussed below.

On the left channel wall in Figure 7, it is seen that most dangling oxygens display a preference for Na^+ ions. On the right channel wall, on the other hand, more preference for Ca^{2+} ions is seen. Single deprotonated silanols did not show consistent preferential adsorption. Clusters of two deprotonated silanols, on the other hand, displayed preferential adsorption for Na^+ ions as shown in II−V and the cluster of

DOI: 10.1021/acs.jpcc.9b02975
J. Phys. Chem. C 2019, 123, 16711−16720

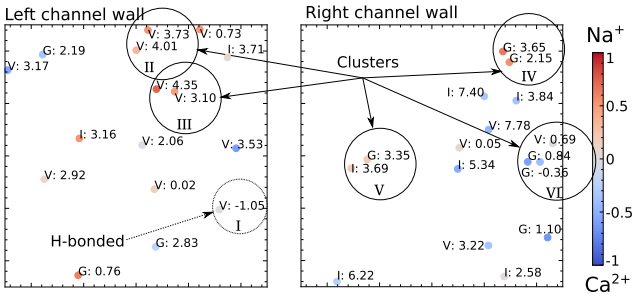

Figure 7. Preferential adsorption of Na^+ (red) and Ca^{2+} (blue) on dangling oxygens on the left and right surfaces of the channel. The letters indicate the type of silanol (i.e., isolated, vicinal, and geminal) and the number a protrusion metric times 100 given by eq 2. Regions I−VI are specifically discussed in the main text. Average PM values for clusters are provided in the additional table within the figure.

three showed preferential adsorption of Ca^{2+} ions as shown in VI.

Upon visual inspection in VMD, it was found that dangling oxygens displaying preferential adsorption of Na^+ ions were frequently submerged into the surface. Furthermore, ions adsorbed to submerged dangling oxygens had a considerably reduced number of water molecules within the first hydration shell (see Table S1 in the SI). Consequently, we argue that steric hindrances to the ion hydration shell exist. This hypothesis was confirmed by introducing a protrusion metric (PM)

$$\mathrm{PM} = \frac{z_{\mathrm{sur}} - z_{\mathrm{O}^-}}{z_{\mathrm{O}^-}} \tag{2}$$

measuring the protrusion of dangling oxygens, as indicated in Figure 3, as a function of their position z_{O^-} with respect to the average z-position of surrounding surface atoms $z_{\mathrm{sur}} = 1/N \sum_k z_k$ within 4.6 Å. A high PM value indicates that a dangling oxygen protrudes from the surface, whereas a low PM value indicates a submerged dangling oxygen. Attempts were made to include also the effect of silanol orientation but failed to produce better results.

The PM is introduced in Figure 7, showing that at low PM, Na^+ is preferentially adsorbed and at high PM, Ca^{2+} is preferentially adsorbed. Exceptions to this finding are indicated with roman numbers. Region I is found without any ion adsorbed due to hydrogen-bonds formed by these dangling oxygens with neighboring silanols. In cases II−VI, on the other hand, multiple dangling oxygens were found next to each other forming clusters, with ions frequently adsorbed to several dangling oxygens simultaneously. Consequently, for these clusters a combined PM, would be indicative for ion-specificity. However, additional factors not included here could play a role in the ion-specificity of clusters. In particular, the following considerations are thought to be relevant: determination of which dangling oxygen is dominant, the distance between dangling oxygens and electrostatic interactions. For example, clusters II, III, IV, and V show similar average PM values, but clusters II, III, and IV show strong preference for Na^+ ions while cluster V shows only a slight preference toward Na^+ ions. Furthermore, cluster VI displays a preference for Ca^{2+} ions despite having a low combined PM value of 0.39/100. In conclusion, for deprotonated silanol clusters, the ion-specificity cannot be explained using only geometric features.

Figure 8 shows that the remaining dangling oxygens (excluding those within I−VI) follow the trend expected by the PM. In Figure 8a, deprotonated silanols that have no other dangling oxygen nearby (henceforth named single) are displayed in blue and those forming clusters (II−VI in Figure 7) in red and yellow. Clusters are shown separately because a different trend is expected for clusters of dangling oxygens compared to single dangling oxygens due to the neglecting of electrostatic contributions by the PM. Preferential Na^+ adsorption is observed at low PM and preferential Ca^{2+} adsorption at large PM. A least squares regression for single dangling oxygens is shown in blue showing a clear trend despite the large spread. At increasing PM, preferential adsorption shifts from Na^+ to Ca^{2+}. For clusters of dangling oxygens, no solid conclusions can be drawn due to the fact that only five data points exist and the results are not consistent with the PM. For single dangling oxygens, however, a clear trend is observed despite the large spread. At increasing PM, preferential adsorption shifts from Na^+ to Ca^{2+}.

We suggest that the trend observed in Figure 8a is related to the number of water molecules within the first hydration shell of adsorbed ions. In fact, in Figure 8b it is observed that the number of water molecules expelled from the first hydration shell of adsorbed ions increases at reducing PM. We argue this to be due to steric hindrances to the first hydration shell of the ion by the structure surrounding dangling oxygen. This hindrance can be overcome by either expelling additional water molecules from the first hydration shell or shifting water molecules within the hydration shell. From Figure 8b, it is seen that consistently more water molecules are expelled from the first hydration shell of Ca^{2+} ions than from that of Na^+ ions. Since Na^+ ions have been found to have a less tight hydration

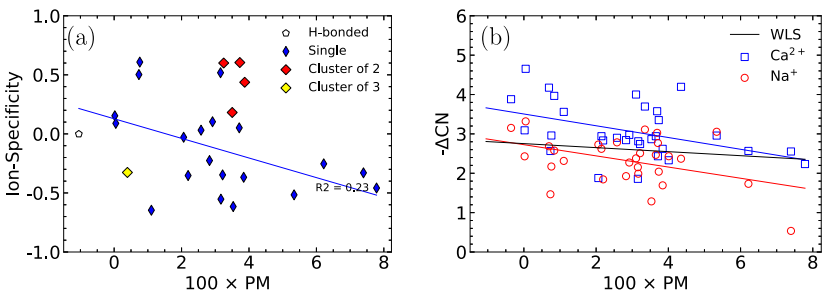

Figure 8. Ion-specificity (a) and reduction in coordination number (b) as a function of PM. Ion-specificity goes from Ca^{2+} preferential adsorption (−1) to Na^+ preferential adsorption (1). Least squares regression is shown to highlight trends for single dangling oxygens (blue) in (a) and −ΔCN for Na^+ (red) and Ca^{2+} (blue) ions in (b). Weighted least squares in (b) shows the trend of −ΔCN for all ions combined, weighted by ion-specificity.

DOI: 10.1021/acs.jpcc.9b02975
J. Phys. Chem. C 2019, 123, 16711−16720

shell, these preferentially adsorb at submerged dangling oxygens by shifting water molecules within their hydration shell.

Additionally, it was found that the adsorption location of Na^+ ions and Ca^{2+} ions on the same dangling oxygen differs. Na^+ ions are frequently found next to dangling oxygen, forming an additional bond with another surface atom or rotating around it, whilst Ca^{2+} ions are almost exclusively found on top of dangling oxygens (see Figure S3 in the SI). This difference in adsorption location can potentially have a large influence on Stern layer dynamics, as adsorbed Na^+ may contribute differently to electro-osmotic or pressure driven flow than adsorbed Ca^{2+} ions. In conclusion, a combination of surface structure-induced ion-specificity and electrostatic attraction, which vary locally over the surface, is ultimately responsible for selectivity.

4. CONCLUSIONS

We have presented a study of ion adsorption, comparing single and mixed electrolytes confined by charged amorphous silica. Ion layering in the Stern layer was evaluated by classifying ions as forming surface CIP and SSIP based on their distance to a given adsorption site. Taking this idea one step further, density profiles were computed for each ionic species as a function of distance to the nearest surface atom, thereby effectively eliminating surface specific roughness effects and obtaining density profiles in line with classical EDL theory. This approach can potentially be used together with EDL models such as the Gouy−Chapman−Stern−Grahame model to improve predictions of the surface or shear plane potentials.

Upon analyzing CIP formation per dangling oxygen, we found surface structure-induced ion-specificity. Although Ca^{2+} ions undergo stronger Coulombic attraction to the negatively charged surface than Na^+ ions, the microstructure of certain adsorption sites may exhibit preference toward Na^+ adsorption by impeding Ca^{2+} ions, which have a tighter hydration shell, from adsorbing. Using this insight, we suggested a simple protrusion metric to predict ion-specificity of dangling oxygens. This metric was shown to work on single dangling oxygens, but failed when multiple dangling oxygens were found close to each other forming clusters. Additional analysis is needed to expand the understanding of the underlying mechanism of this ion-specificity and test the applicability of the protrusion metric with other electrolytes and oxide surfaces. We expect this metric to be especially successful in mixed electrolytes containing counterions of the same valency but dissimilar hydration properties.

In conclusion, surface roughness, as well as the placement of deprotonated silanols, will have a severe impact on preferential adsorption, related to the steric hindrance for ion hydration shells. This finding can be used to microengineer surfaces with selectivities for specific ions for purposes ranging from water desalination to osmotic power harvesting. Furthermore, insight into the relationship between the surface structure and preferential adsorption can help understand experimental results.

ASSOCIATED CONTENT

Supporting Information

The Supporting Information is available free of charge on the ACS Publications website at DOI: 10.1021/acs.jpcc.9b02975.

Additional figures and tables, computational details, amorphous silica characterization, uncertainty quantification, symmetrization of results, data files for all systems, amorphous SiO_2 data files and LAMMPS scripts for the 0.3Na0.3Ca system; a versatile Python-based library for the creation of various shapes of amorphous silica interfaces with electrolyte solutions is available on request via GitLab (PDF)

AUTHOR INFORMATION

Corresponding Author

*E-mail: r.m.hartkamp@tudelft.nl.

ORCID

Othonas A. Moultos: 0000-0001-7477-9684
Bertrand Siboulet: 0000-0002-6895-202X
Johan T. Padding: 0000-0003-4161-0748
Remco Hartkamp: 0000-0001-8746-8244

Notes

The authors declare no competing financial interest.

ACKNOWLEDGMENTS

This work was carried out on the Dutch national e-infrastructure with the support of SURF Cooperative.

REFERENCES

(1) Eijkel, J. C.; van den Berg, A. Nanofluidics: What Is It and What Can We Expect from It? *Microfluid. Nanofluid.* **2005**, *1*, 249−267.
(2) Prakash, S.; Piruska, A.; Gatimu, E. N.; Bohn, P. W.; Sweedler, J. V.; Shannon, M. A. Nanofluidics: Systems and Applications. *IEEE Sens. J.* **2008**, *8*, 441−450.
(3) Bourg, I. C.; Sposito, G. Molecular Dynamics Simulations of the Electrical Double Layer on Smectite Surfaces Contacting Concentrated Mixed Electrolyte (NaCl-$CaCl_2$) Solutions. *J. Colloid Interface Sci.* **2011**, *360*, 701−715.
(4) Ong, S.; Zhao, X.; Eisenthal, K. B. Polarization of Water Molecules at a Charged Interface: Second Harmonic Studies of the Silica/Water Interface. *Chem. Phys. Lett.* **1992**, *191*, 327−335.
(5) Patwardhan, S. V.; Emami, F. S.; Berry, R. J.; Jones, S. E.; Naik, R. R.; Deschaume, O.; Heinz, H.; Perry, C. C. Chemistry of Aqueous Silica Nanoparticle Surfaces and the Mechanism of Selective Peptide Adsorption. *J. Am. Chem. Soc.* **2012**, *134*, 6244−6256.
(6) Rancan, F.; Gao, Q.; Graf, C.; Troppens, S.; Hadam, S.; Hackbarth, S.; Kembuan, C.; Blume-Peytavi, U.; Rühl, E.; Lademann, J.; et al. Skin Penetration and Cellular Uptake of Amorphous Silica Nanoparticles with Variable Size, Surface Functionalization, and Colloidal Stability. *ACS Nano* **2012**, *6*, 6829−6842.
(7) Corno, M.; Delle Piane, M.; Choquet, P.; Ugliengo, P. Models for Biomedical Interfaces: a Computational Study of Quinone-Functionalized Amorphous Silica Surface Features. *Phys. Chem. Chem. Phys.* **2017**, *19*, 7793−7806.
(8) Rimola, A.; Costa, D.; Sodupe, M.; Lambert, J.-F.; Ugliengo, P. Silica Surface Features and Their Role in the Adsorption of Biomolecules: Computational Modeling and Experiments. *Chem. Rev.* **2013**, *113*, 4216−4313.
(9) Liu, N.; Liu, Y. H.; Feng, P.; Qiang Zhu, L.; Shi, Y.; Wan, Q. Enhancing the pH Sensitivity by Laterally Synergic Modulation in Dual-Gate Electric-Double-Layer Transistors. *Appl. Phys. Lett.* **2015**, *106*, No. 073507.
(10) Sivakumarasamy, R.; Hartkamp, R.; Siboulet, B.; Dufrêche, J. F.; Nishiguchi, K.; Fujiwara, A.; Clément, N. Selective Layer-Free Blood Serum Ionogram Based on Ion-Specific Interactions with a Nanotransistor. *Nat. Mater.* **2018**, *17*, 464−470.
(11) Lützenkirchen, J.; Preočanin, T.; Kovačević, D.; Tomišić, V.; Lövgren, L.; Kallay, N. Potentiometric Titrations as a Tool for Surface Charge Determination. *Croat. Chem. Acta* **2012**, *85*, 391−417.

DOI: 10.1021/acs.jpcc.9b02975
J. Phys. Chem. C 2019, 123, 16711−16720

(12) Kosmulski, M. The pH-Dependent Surface Charging and the Points of Zero Charge. *J. Colloid Interface Sci.* **2002**, *253*, 77−87.
(13) Grahame, D. C. The Electrical Double Layer and the Theory of Electrocapillarity. *Chem. Rev.* **1947**, *41*, 441−501.
(14) Hartkamp, R.; Biance, A. L.; Fu, L.; Dufrêche, J. F.; Bonhomme, O.; Joly, L. Measuring Surface Charge: Why Experimental Characterization and Molecular Modeling Should be Coupled. *Curr. Opin. Colloid Interface Sci.* **2018**, *37*, 101−114.
(15) Argyris, D.; Tummala, N. R.; Striolo, A.; Cole, D. R. Molecular Structure and Dynamics in Thin Water Films at the Silica and Graphite Surfaces. *J. Phys. Chem. C* **2008**, *112*, 13587−13599.
(16) Argyris, D.; Cole, D. R.; Striolo, A. Dynamic Behavior of Interfacial Water at the Silica Surface. *J. Phys. Chem. C* **2009**, *113*, 19591−19600.
(17) Hassanali, A. A.; Singer, S. J. Static and Dynamic Properties of the Water/Amorphous Silica Interface: a Model for the Undissociated Surface. *J. Comput.-Aided Mater. Des.* **2007**, *14*, 53−63.
(18) Hassanali, A. A.; Singer, S. J. Model for the Water-Amorphous Silica Interface: The Undissociated Surface. *J. Phys. Chem. B* **2007**, *111*, 11181−11193.
(19) Bourg, I. C.; Steefel, C. I. Molecular Dynamics Simulations of Water Structure and Diffusion in Silica Nanopores. *J. Phys. Chem. C* **2012**, *116*, 11556−11564.
(20) Collin, M.; Gin, S.; Dazas, B.; Mahadevan, T.; Du, J.; Bourg, I. C. Molecular Dynamics Simulations of Water Structure and Diffusion in a 1 nm Diameter Silica Nanopore as a Function of Surface Charge and Alkali Metal Counterion Identity. *J. Phys. Chem. C* **2018**, *122*, 17764−17776.
(21) Lorenz, C. D.; Travesset, A. Charge Inversion of Divalent Ionic Solutions in Silica Channels. *Phys. Rev. E* **2007**, *75*, No. 061202.
(22) Lorenz, C. D.; Crozier, P. S.; Anderson, J. A.; Travesset, A. Molecular Dynamics of Ionic Transport and Electrokinetic Effects in Realistic Silica Channels. *J. Phys. Chem. C* **2008**, *112*, 10222−10232.
(23) Haria, N. R.; Lorenz, C. D. Ion Exclusion and Electrokinetic Effects Resulting from Electro-Osmotic Flow of Salt Solutions in Charged Silica Nanopores. *Phys. Chem. Chem. Phys.* **2012**, *14*, 5935−5944.
(24) Haria, N. R.; Lorenz, C. D. Atomistic Description of Pressure-Driven Flow of Aqueous Salt Solutions through Charged Silica Nanopores. *J. Phys. Chem. C* **2015**, *119*, 12298−12311.
(25) Zhang, H.; Hassanali, A. A.; Shin, Y. K.; Knight, C.; Singer, S. J. The Water-Amorphous Silica Interface: Analysis of the Stern Layer and Surface Conduction. *J. Chem. Phys.* **2011**, *134*, No. 024705.
(26) Ho, T. A.; Argyris, D.; Cole, D. R.; Striolo, A. Aqueous NaCl and CsCl Solutions Confined in Crystalline Slit-Shaped Silica Nanopores of Varying Degree of Protonation. *Langmuir* **2012**, *28*, 1256−1266.
(27) Bourg, I. C.; Lee, S. S.; Fenter, P.; Tournassat, C. Stern Layer Structure and Energetics at Mica-Water Interfaces. *J. Phys. Chem. C* **2017**, *121*, 9402−9412.
(28) Hocine, S.; Hartkamp, R.; Siboulet, B.; Duvail, M.; Coasne, B.; Turq, P.; Dufrêche, J. F. How Ion Condensation Occurs at a Charged Surface: A Molecular Dynamics Investigation of the Stern Layer for Water-Silica Interfaces. *J. Phys. Chem. C* **2016**, *120*, 963−973.
(29) Hartkamp, R.; Siboulet, B.; Dufrêche, J. F.; Coasne, B. Ion-Specific Adsorption and Electroosmosis in Charged Amorphous Porous Silica. *Phys. Chem. Chem. Phys.* **2015**, *17*, 24683−24695.
(30) Prakash, S.; Zambrano, H. A.; Rangharajan, K. K.; Rosenthal-Kim, E.; Vasquez, N.; Conlisk, A. T. Electrokinetic Transport of Monovalent and Divalent Cations in Silica Nanochannels. *Microfluid. Nanofluid.* **2016**, *20*, 8.
(31) Qiu, Y.; Chen, Y. Counterions and Water Molecules in Charged Silicon Nanochannels: the Influence of Surface Charge Discreteness. *Mol. Simul.* **2015**, *41*, 1187−1192.
(32) Chen, M.; Jiang, D.; Jiang, K.; Qiu, Y. Investigation of Charge Inversion in Silicon Nanochannels with Molecular Dynamics Simulation. *Proc. Inst. Mech. Eng., Part N* **2016**, *230*, 51−54.
(33) Sam, A.; Kannam, S. K.; Hartkamp, R.; Sathian, S. P. Water Flow in Carbon Nanotubes: The Effect of Tube Flexibility and Thermostat. *J. Chem. Phys.* **2017**, *146*, No. 234701.
(34) Besteman, K.; Zevenbergen, M. A.; Heering, H. A.; Lemay, S. G. Direct Observation of Charge Inversion by Multivalent Ions as a Universal Electrostatic Phenomenon. *Phys. Rev. Lett.* **2004**, *93*, No. 170802.
(35) van der Heyden, F. H. J.; Stein, D.; Besteman, K.; Lemay, S. G.; Dekker, C. Charge Inversion at High Ionic Strength Studied by Streaming Currents. *Phys. Rev. Lett.* **2006**, *96*, No. 224502.
(36) Rijnaarts, T.; Huerta, E.; van Baak, W.; Nijmeijer, K. Effect of Divalent Cations on RED Performance and Cation Exchange Membrane Selection to Enhance Power Densities. *Environ. Sci. Technol.* **2017**, *51*, 13028−13035.
(37) Adapa, S.; Malani, A. Role of Hydration Energy and Co-ions Association on Monovalent and Divalent Cations Adsorption at Mica-Aqueous Interface. *Sci. Rep.* **2018**, *8*, No. 12198.
(38) Wang, Z. Y.; Zhang, P.; Ma, Z. On the physics of both surface overcharging and charge reversal at heterophase interfaces. *Phys. Chem. Chem. Phys.* **2018**, *20*, 4118−4128.
(39) van Beest, B. W. H.; Kramer, G. J.; van Santen, R. A. Force Fields for Silicas and Aluminophosphates Based on Ab Initio Calculations. *Phys. Rev. Lett.* **1990**, *64*, 1955−1958.
(40) Vollmayr, K.; Kob, W.; Binder, K. Cooling-Rate Effects in Amorphous Silica: A Computer-Simulation Study. *Phys. Rev. B: Condens. Matter Mater. Phys.* **1996**, *54*, 15808−15827.
(41) Geske, J.; Vogel, M. Creating Realistic Silica Nanopores for Molecular Dynamics Simulations. *Mol. Simul.* **2017**, *43*, 13−18.
(42) Mozzi, R. L.; Warren, B. E. The Structure of Vitreous Silica. *J. Appl. Crystallogr.* **1969**, *2*, 164−172.
(43) Konnert, J. H.; Karle, J. The Computation of Radial Distribution Functions for Glassy Materials. *Acta Crystallogr., Sect. A: Found. Adv.* **1973**, *29*, 702−710.
(44) Grimley, D. I.; Wright, A. C.; Sinclair, R. N. Neutron Scattering from Vitreous Silica IV. Time-of-Flight Diffraction. *J. Non-Cryst. Solids* **1990**, *119*, 49−64.
(45) Emami, F. S.; Puddu, V.; Berry, R. J.; Varshney, V.; Patwardhan, S. V.; Perry, C. C.; Heinz, H. Force Field and a Surface Model Database for Silica to Simulate Interfacial Properties in Atomic Resolution. *Chem. Mater.* **2014**, *26*, 2647−2658.
(46) Halbert, S.; Ispas, S.; Raynaud, C.; Eisenstein, O. Modelling the Surface of Amorphous Dehydroxylated Silica: The Influence of the Potential on the Nature and Density of Defects. *New J. Chem.* **2018**, *42*, 1356−1367.
(47) Zhuravlev, L. T. The Surface Chemistry of Amorphous Silica. Zhuravlev model. *Colloids Surf., A* **2000**, *173*, 1−38.
(48) Ugliengo, P.; Sodupe, M.; Musso, F.; Bush, I. J.; Orlando, R.; Dovesi, R. Realistic Models of Hydroxylated Amorphous Silica Surfaces and MCM- 41 Mesoporous Material Simulated by Large-Scale Periodic B3LYP Calculations. *Adv. Mater.* **2008**, *20*, 4579−4583.
(49) Garofalini, S. H. Molecular Dynamics Computer Simulations of Silica Surface Structure and Adsorption of Water Molecules. *J. Non-Cryst. Solids* **1990**, *120*, 1−12.
(50) Comas-Vives, A. Amorphous SiO_2 Surface Models: Energetics of the Dehydroxylation Process, Strain, Ab Initio Atomistic Thermodynamics and IR Spectroscopic Signatures. *Phys. Chem. Chem. Phys.* **2016**, *18*, 7475−7482.
(51) Ewen, J. P.; Gao, H.; Müser, M. H.; Dini, D. Shear Heating, Flow, and Friction of Confined Molecular Fluids at High Pressure. *Phys. Chem. Chem. Phys.* **2019**, *21*, 5813−5823.
(52) Yeh, I. C.; Berkowitz, M. L. Ewald Summation for Systems with Slab Geometry. *J. Chem. Phys.* **1999**, *111*, 3155−3162.
(53) Abascal, J. L.; Vega, C. A General Purpose Model for the Condensed Phases of Water: TIP4P/2005. *J. Chem. Phys.* **2005**, *123*, No. 234505.
(54) Joung, I. S.; Cheatham, T. E. Determination of Alkali and Halide Monovalent Ion Parameters for Use in Explicitly Solvated Biomolecular Simulations. *J. Phys. Chem. B* **2008**, *112*, 9020−9041.

DOI: 10.1021/acs.jpcc.9b02975
J. Phys. Chem. C 2019, 123, 16711−16720

(55) Mamatkulov, S.; Fyta, M.; Netz, R. R. Force Fields for Divalent Cations Based on Single-Ion and Ion-Pair Properties. *J. Chem. Phys.* **2013**, *138*, No. 024505.
(56) Cygan, R. T.; Liang, J.-J.; Kalinichev, A. G. Molecular Models of Hydroxide, Oxyhydroxide, and Clay Phases and the Development of a General Force Field. *J. Phys. Chem. B* **2004**, *108*, 1255−1266.
(57) Pouvreau, M.; Greathouse, J. A.; Cygan, R. T.; Kalinichev, A. G. Structure of Hydrated Gibbsite and Brucite Edge Surfaces: DFT Results and Further Development of the ClayFF Classical Force Field with Metal-O-H Angle Bending Terms. *J. Phys. Chem. C* **2017**, *121*, 14757−14771.
(58) Mishra, R. K.; Mohamed, A. K.; Geissbühler, D.; Manzano, H.; Jamil, T.; Shahsavari, R.; Kalinichev, A. G.; Galmarini, S.; Tao, L.; Heinz, H.; et al. cemff: A Force Field Database for Cementitious Materials Including Validations, Applications and Opportunities. *Cem. Concr. Res.* **2017**, *102*, 68−89.
(59) Vega, C.; Abascal, J. L. Simulating Water with Rigid Non-Polarizable Models: A General Perspective. *Phys. Chem. Chem. Phys.* **2011**, *13*, 19663−19688.
(60) Ryckaert, J. P.; Ciccotti, G.; Berendsen, H. J. Numerical Integration of the Cartesian Equations of Motion of a System with Constraints: Molecular Dynamics of n-Alkanes. *J. Comput. Phys.* **1977**, *23*, 327−341.
(61) Plimpton, S. Fast Parallel Algorithms for Short-Range Molecular Dynamics. *J. Comput. Phys.* **1995**, *117*, 1−19.
(62) Brown, M. A.; Goel, A.; Abbas, Z. Effect of Electrolyte Concentration on the Stern Layer Thickness at a Charged Interface. *Angew. Chem., Int. Ed.* **2016**, *55*, 3790−3794.
(63) Hartkamp, R.; Coasne, B. Structure and Transport of Aqueous Electrolytes: From Simple Halides to Radionuclide Ions. *J. Chem. Phys.* **2014**, *141*, No. 124508.
(64) Rahnemaie, R.; Hiemstra, T.; van Riemsdijk, W. H. A New Surface Structural Approach to Ion Adsorption: Tracing the Location of Electrolyte Ions. *J. Colloid Interface Sci.* **2006**, *293*, 312−321.
(65) Lyklema, J. Nomenclature, Symbols, Definitions and Measurements for Electrified Interfaces in Aqueous Dispersions of Solids (Recommendations 1991). *Pure Appl. Chem.* **1991**, *63*, 895−906.
(66) Henke, L.; Nagy, N.; Krull, U. J. An AFM Determination of the Effects on Surface Roughness Caused by Cleaning of Fused Silica and Glass Substrates in the Process of Optical Biosensor Preparation. *Biosens. Bioelectron.* **2002**, *17*, 547−555.
(67) Rezaei, M.; Azimian, A. R.; Pishevar, A. R.; Bonthuis, D. J. Viscous Interfacial Layer Formation Causes Electroosmotic Mobility Reversal in Monovalent Electrolytes. *Phys. Chem. Chem. Phys.* **2018**, *20*, 22517−22524.
(68) Celebi, A.; Beskok, A. Molecular and Continuum Transport Perspectives on Electroosmotic Slip Flows. *J. Phys. Chem. C* **2018**, *122*, 9699−9709.
(69) ben Jabrallah, S.; Malloggi, F.; Belloni, L.; Girard, L.; Novikov, D.; Mocuta, C.; Thiaudière, D.; Daillant, J. Electrolytes at Interfaces: Accessing the First Nanometers Using X-ray Standing Waves. *Phys. Chem. Chem. Phys.* **2017**, *19*, 167−174.
(70) Lis, D.; Backus, E. H. G.; Hunger, J.; Parekh, S. H.; Bonn, M. Liquid Flow Along a Solid Surface Reversibly Alters Interfacial Chemistry. *Science* **2014**, *344*, 1138−1142.
(71) Lian, C.; Xian, K.; Liu, H.; Wu, J. Flow Effects on Silicate Dissolution and Ion Transport at an Aqueous Interface. *Phys. Chem. Chem. Phys.* **2019**, *21*, 6970−6975.
(72) Siboulet, B.; Hocine, S.; Hartkamp, R.; Dufrêche, J. F. Scrutinizing Electro-Osmosis and Surface Conductivity with Molecular Dynamics. *J. Phys. Chem. C* **2017**, *121*, 6756−6769.
(73) Squires, T. M.; Bazant, M. Z. Induced-Charge Electro-Osmosis. *J. Fluid Mech.* **2004**, *509*, 217−252.
(74) Sadr, R.; Yoda, M.; Zheng, Z.; Conlisk, A. T. An Experimental Study of Electro-Osmotic Flow in Rectangular Microchannels. *J. Fluid Mech.* **2004**, *506*, 357−367.
(75) Grosberg, A. Y.; Nguyen, T. T.; Shklovskii, B. I. Colloquium: The Physics of Charge Inversion in Chemical and Biological Systems. *Rev. Mod. Phys.* **2002**, *74*, 329−345.
(76) Chen, Y.; Ni, Z.; Wang, G.; Xu, D.; Li, D. Electroosmotic Flow in Nanotubes with High Surface Charge Densities. *Nano Lett.* **2008**, *8*, 42−48.
(77) Dewan, S.; Carnevale, V.; Bankura, A.; Eftekhari-Bafrooei, A.; Fiorin, G.; Klein, M. L.; Borguet, E. Structure of Water at Charged Interfaces: A Molecular Dynamics Study. *Langmuir* **2014**, *30*, 8056−8065.
(78) Kohagen, M.; Mason, P. E.; Jungwirth, P. Accurate Description of Calcium Solvation in Concentrated Aqueous Solutions. *J. Phys. Chem. B* **2014**, *118*, 7902−7909.
(79) Quesada-Pérez, M.; González-Tovar, E.; Martín-Molina, A.; Lozada-Cassou, M.; Hidalgo-Álvarez, R. Overcharging in Colloids: Beyond the Poisson-Boltzmann Approach. *ChemPhysChem* **2003**, *4*, 234−248.
(80) Lenz, O.; Holm, C. Simulation of Charge Reversal in Salty Environments: Giant Overcharging? *Eur. Phys. J. E* **2008**, *26*, 191−195.
(81) Semenov, I.; Raafatnia, S.; Sega, M.; Lobaskin, V.; Holm, C.; Kremer, F. Electrophoretic Mobility and Charge Inversion of a Colloidal Particle Studied by Single-Colloid Electrophoresis and Molecular Dynamics Simulations. *Phys. Rev. E: Stat., Nonlinear, Soft Matter Phys.* **2013**, *87*, No. 022302.
(82) Li, R.; Todd, B. A. Multivalent Ion Screening of Charged Glass Surface Studied by Streaming Potential Measurements. *J. Chem. Phys.* **2013**, *139*, No. 194704.

DOI: 10.1021/acs.jpcc.9b02975
J. Phys. Chem. C 2019, 123, 16711−16720